RSC Advances

Spectral weight shift in valence band density of states and concurrent increase in field emission by hydrogenation of FeCo-SiO2 nanocomposites

Journal:	*RSC Advances*
Manuscript ID:	RA-ART-04-2015-006106.R1
Article Type:	Paper
Date Submitted by the Author:	27-Jun-2015

Complete List of Authors:	Sarker, Debalaya; Indian Institute of Technology Delhi, Physics Ghosh, S; Indian Institute of Technology Delhi, Physics Srivastava, Pankaj; Indian Institute of Technology Delhi, Physics

SCHOLARONE™
Manuscripts

Journal Name RSCPublishing

ARTICLE

Cite this: DOI: 10.1039/x0xx00000x

Received 00th January 2012,
Accepted 00th January 2012

DOI: 10.1039/x0xx00000x

www.rsc.org/

Spectral weight shift in valence band density of states and concurrent increase in field emission by hydrogenation of FeCo-SiO_2 nanocomposites

Debalaya Sarker,[a] S. Ghosh[a], and P. Srivastava[a]

Hydrogenated and roughened surface of hydrogen plasma treated (HPT) FeCo-SiO_2 nanogranular films are found to be efficient field emitters in comparison to their as grown and furnace annealed counterparts. Partial etching by hydrogen plasma roughens the surface and improves the field emission by enhancing the local electric field at the protrusion tips. A layer of $Fe^{\delta+}$–$H^{\delta-}$ dipoles over the roughened HPT film surface and enhanced defects are likely to make the composite surface more emission-active by reducing the overall work function. The reconstruction of the electronic structure is mainly attributed to the Fe^{2+} to Fe^{3+} conversion, appearance of anti-bonding states together with hydrogen-induced volume expansion. Tunnelling of electrons from valence band becomes easier *via* these inter-gap anti-bonding states. The agglomeration of nanoparticles, out-diffusion of hydrogen and further etching of the film at higher substrate temperature of plasma treated films reduces the FE current density drastically.

Introduction

Several advantages such as high brightness, fast response, low power consumption and many more have ascertained field emission (FE) of electrons as an emerging research area in recent past.[1,2] On application of very high electric field (~10-50 V/μm) electrons from conducting/semiconducting materials get ejected via quantum mechanical tunnelling through the surface potential barrier. High aspect ratio (height to radius ratio) of one dimensional nanomaterials like carbon nanotubes (CNTs), nanorods of different materials like Si, tungsten oxide, ZnO, Co_3O_4 renders exceptionally good FE properties like high current density, low turn on and threshold fields. [3-7] Different 2D materials viz. graphene[8], ZnO[9] *etc*. are known for their atomically thin planar structure, which are applicable in flat display technologies. Mechanical durability, temporal stability, smaller dimension are among several advantages of planar emitters over the one dimensional field emitting surface structures. Invoked by the planar type design, many groups have proposed different planar field emitters made with nanocomposites consisting of metal nanoparticles embedded in dielectric matrix, such as Ag-SiO_2,[10] Co-SiO_2, SiC,[11] WS2-RGO ,[12] Ni-SiO_2[13,14] *etc*. In our previous studies changes in field emission properties of Ni-SiO_2 nanocomposites, by modifying their surface morphology, band structure, density of sates (DOS) employing annealing treatment and swift heavy ion irradiation are reported.[13,14] The FeCo alloy has lower work function and lesser possibility of getting oxidized in comparison to individual Fe/ Co. Thus stable FeCo nanoparticles[15,16] embedded in SiO_2 matrix can act as a promising field emitter.

Insertion of different elements like N, Ar or H in field emitting materials has been proven to improve their emission properties by introducing defects within the field emitters as well as by creating new emitting sites on the emitter surfaces and reducing the effective work function of the emitting material.[17] Among various surface treatments, treating with H-plasma at different conditions can result in improvement of FE properties of ZnO,[18] CNTs [19] due to enhancement of the surface conductivity. Zhu *et al*. have shown that, H-plasma annealing reduces electron affinity of the surface of diamond films.[20] Sugino *et al.* [21] acredited the plasma induced surface roughness for better FE properties of GaN films. Bangmin Zhang et al. have reported high resistivity of FeCoNiNbB–SiO_2 nano-granular films in reference 22. We tried to improve the conductivity of the FeCo-SiO_2 nanogranular films by H-plasma treatment here. The agglomeration and growth of metal nanoparticles in SiO_2 matrix by furnace annealing can provide

This journal is © The Royal Society of Chemistry 2013

proper emission sites within metal-insulator nanogranular films.[14] Because of high conductivity of the metal nanoparticles with respect to surrounding insulating media, electrons find their transportation path through metal nanoparticles out of the film surface plane as the metal-insulator-metal structure restricts the planar motion of the same.

In this letter, we report the FE study of $FeCo-SiO_2$ nanocomposite thin films treated with hydrogen plasma and annealed in hydrogen gas environment at different temperatures. An attempt has been made here to understand the underlying mechanism behind enhancement of emission current from plasma treated surface of bimetallic $FeCo-SiO_2$ nanocomposite by studying x-ray photoelectron spectroscopy (XPS), atomic force microscopy (AFM), conducting AFM (CAFM), and elastic recoil detection analysis (ERDA) in detail. The improved FE properties are mainly attributed to appearance of anti-bonding states near Fermi level, increased emission sites and plasma induced surface protrusions along with volume expansion of metal nano-clusters.

Experimental Details:

Fe and Co foils were co-sputtered by neutral Ar atoms with SiO_2 for the synthesis of $FeCo-SiO_2$ nanocomposite films by fast atom beam (FAB) sputtering technique as described in our earlier work.[15] The content of metallic nanoparticles in the composite was kept ~20% as per calculation based on area fraction and sputtering yield.[23] A set of as prepared samples (AD) were then subjected to tubular furnace annealing in hydrogen gas environment for 2 hours at 200°C and 350°C and named as 200AN and 350AN. Another set of AD samples were treated with hydrogen plasma, generated by rf power (in PECVD SAMCO-PD2S) for 45 minutes at two different substrate temperatures (200°C and 350°C). These samples are named as HPT200 and HPT350. During H-plasma annealing, chamber pressure was kept at 2.0 mbar with a constant H flow rate of 10 sccm and constant rf power of 25 W. The x-ray photoelectron spectroscopy (XPS) measurements were performed using SPECS system with Mg K_α source ($h\upsilon$ =1253.6 eV) in a base pressure below $1x10^{-9}$ mbar. AFM and CAFM (Dimension Icon Model, Bruker) were performed to examine the surface morphology and conductivity of the films respectively. Kelvin probe measurements were carried out with (KP technology, KP020) having gold probe as a reference to enumerate the work function of the surface. Finally, field emission measurements were carried out in a high vacuum chamber (7.5×10^{-7} mbar) using diode geometry. Details of the same are given in our previous publications.[13,24] The distance between sample, used as a cathode, and steel plate anode was kept fixed at 200 μm for all measurements. Applied electric field was varied from 1.75 V/μm to 15V/ μm with APLAB power source (H5KO2N) and the emission current was recorded with Keithley 2616. The amount of hydrogen incorporated in the films by the hydrogen plasma treatment was characterized by ERDA technique with Ag^{+7} ions of 100 MeV, using the 15UD pelletron accelerator of Inter University Accelerator Centre (IUAC), New Delhi.

Result and Discussion:

Cold field emission, being a surface phenomenon, will largely be affected by the work function of the emitting material. Kelvin probe measurement ensures the lowest work function of 200HPT film (table 1) among all studied here. The current density J of a field emitter is related to applied field E by FN equation.[25]

$$J = A\frac{aE^2\beta^2}{\varphi}\exp\left(-\frac{b\varphi^{\frac{3}{2}}}{\beta E}\right) \qquad (1)$$

Where A = effective emissive area factor defined by ratio of effective emissive area and total sample area, $a = \frac{e^3}{8\pi h_p} =$ 1.54434×10^{-6} A.eV.V^{-2} and $b = \frac{8\pi}{3}.\frac{(2m_e)^{1/2}}{eh_p} = 6.83\times10^7$ V.eV$^{-3/2}$.cm^{-1} are constants, β is field enhancement factor and φ is the work function of material. The emission current density (J) versus applied electric field (E) plots for all films are shown in figure 1. It is evident that HPT200 film is the best field emitter among all with a maximum current density of ~55 μA/cm² and minimum turn on and threshold fields as tabulated in figure1. With the increment of the furnace annealing temperature in H_2 environment, J is observed to increase till 200°C, and with further increase in temperature to 350°C, the same diminishes due to agglomeration of particles inside insulating matrix.

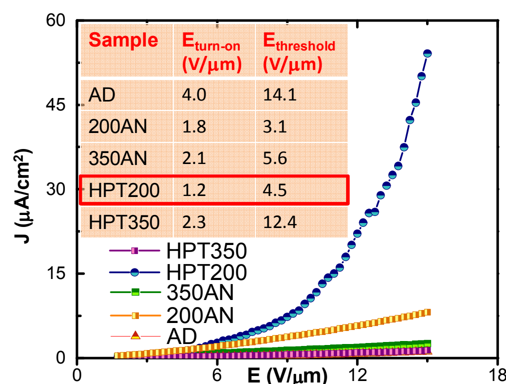

Figure:1 J vs. E plots for all films, indicating highest emission current in HPT 200 film.

To understand the effect of H incorporation on FE properties ERDA measurements were carried out on plasma treated and annealed films. A fluence dependent areal concentration for different films is analysed using standard formulation of ERDA[26] and is plotted in Fig 2. The HPT200 film contains maximum H. The atomic H thus causes expansion of FeCo nano-clusters volume and improves the electrical conduction through insulating matrix. As we increase the plasma annealing temperature to 350°C, H content reduces due to out-diffusion of

This journal is © The Royal Society of Chemistry 2012

H at higher temperature, which explains its inferior FE characteristics. The 200AN film also contains considerable amount of H but does not emit electrons sufficiently because of adsorbed oxygen on surface and less surface roughness (discussed later). Also annealing in H_2 environment might have modified the size of the particles but formation of dipole layer (discussed later) is not likely in this case as in the case of plasma treatment where atomic H form Fe-H or Co-H bonds.

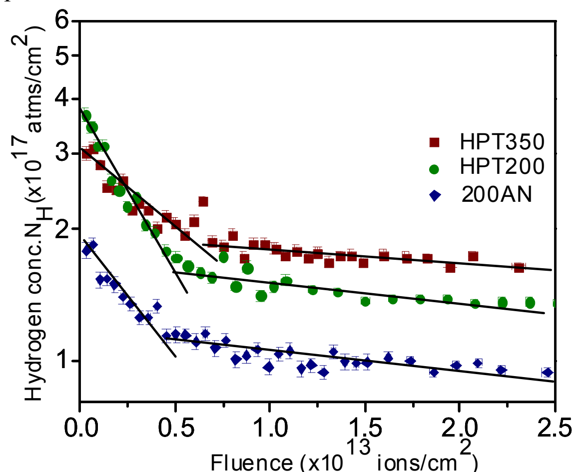

Figure 2: H counts from ERDA measurements as a function of incident ion fluence.

The 3D AFM images of AD and HPT200 films in figure 3(a) show the surface protrusions are formed after plasma treatment. Figure 3(b) shows the AFM and CAFM images of HPT200 and 200AN films. The number of particles versus calculated effective emissive area (conducting above 0.45 nA) and particle diameter plots are shown in the insets. Though the effective emissive area of the HPT200 film (1.7%) within the scanned domain is lesser than that of 200AN film (2.0%), the r.m.s surface roughness of the HPT200 film is the highest among all (see table 1). Also the efficiency of plasma treatment in nanoparticle growth in comparison with the furnace annealing is evident from the larger average particle diameter in HPT200 film (~10 nm) over the sample surface.

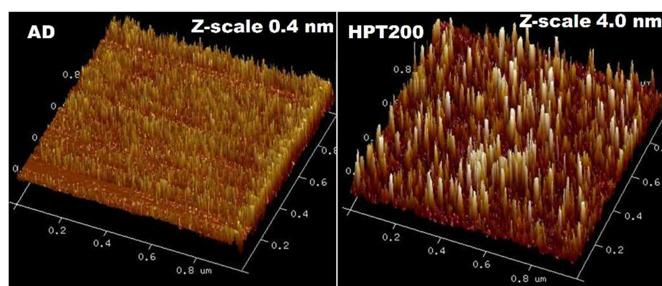

Figure 3(a): 3D AFM images of AD and HPT200 films.

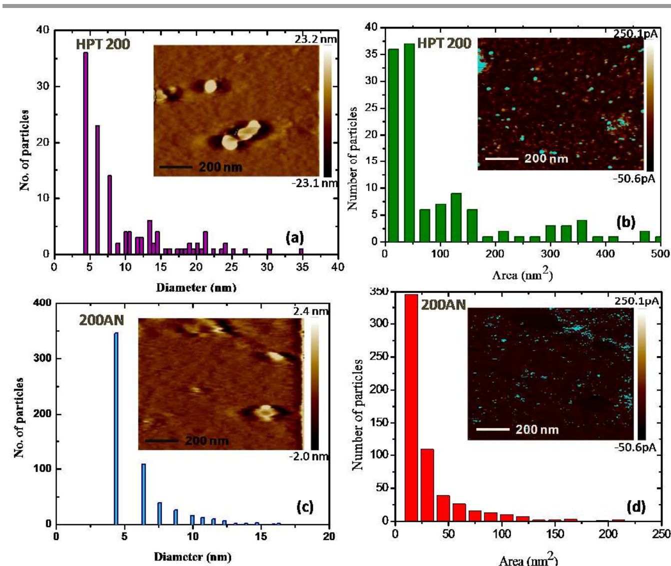

Figure 3(b): AFM and CAFM images and corresponding size and conducting area distribution of HPT200 and 200AN films.

It is clearly evident that FE depends on reconstruction of electronic structure due to hydrogenation; key issue being the modified electronic structure near Fermi level. KP measurement shows the lowest work function, implying highest VB DOS for the HPT200 film (table 1). Spin polarization of 3d orbital gets weakened due to occupation by hydrogen. 3d density of states (DOS) is more occupied due to hydrogenation if an unchanged profile of the 3d DOS is assumed. This model is the so-called “rigid d-band model”. [27] To have an insight of the changes in valence band DOS, XPS valance band spectra of AD, 200AN and HPT200 films are analysed (figure 4(a)). Figure 4(b) shows the Fe 2p XPS spectra of these films.. Schrantz et al. [28] have reported that 1.5 eV, 3 eV and 5.5 eV peaks are indicative of O 2p-Fe 3d hybridization states and O 2p valence states respectively. In the present case, 3d metallic states have contributions from both Fe and Co. VB of HPT200 film shows emergence of more 3d-like or, metallic anti-bonding states near Fermi level, causing shift of VB edge towards lower B.E (figure 4(a)). Fe 2p core level (figure 4(b)) supports Fe^{2+} to energetically higher Fe^{3+} conversion taking into account the charge-transfer theory.[29] The gradual reduction in Fe^{2+} peak, as one goes from as deposited to furnace annealed and plasma annealed film, demonstrates the efficiency of plasma treatment in reducing Fe. Atomic H plays an important role in modifying the electronic state of Fe/Co due to its electron affinity as:

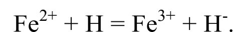

$$Fe^{2+} + H = Fe^{3+} + H^-.$$

Changed electronic states have resulted by splitting of d orbital due to Fe-H / Co-H bonding and anti-bonding, which is evident from VB XPS (figure 4). A shift in Fermi energy towards lower energy along with the rise of anti-bonding states near Fermi level in the HPT200 film is schematically shown in figure 5, which further reduces the required energy for electron emission by step wise hopping of electrons.

This journal is © The Royal Society of Chemistry 2012

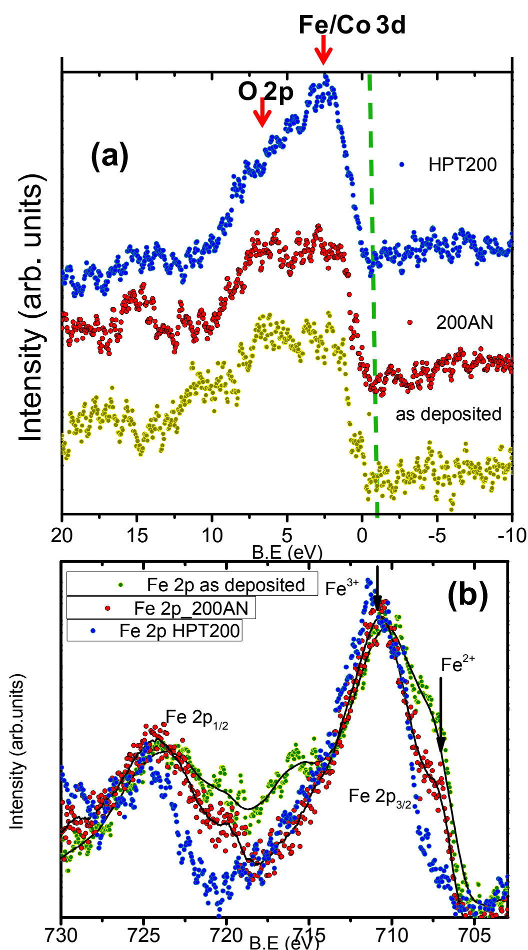

Figure 4: (a) XPS valence band spectrum and (b) Fe 2p spectrum for AD, 200AN, HPT200 films

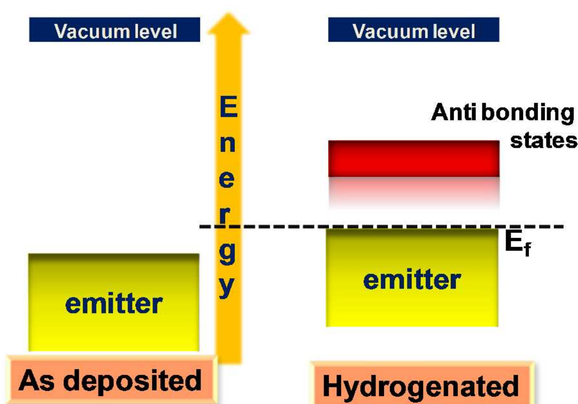

Figure 5: Schemtic of Fermi energy shift and anti-bonding states formation after hydrogenation.

These split states reduce the effective tunnelling step barrier further and provide path to the electron to get easily knocked off the surface. Also, the H atom in the interstitial space has caused volume expansion resulting in narrow 3*d* band. The emission of electron through plasma treated composite surface is shown schematically in figure 6. The dipoles have caused band bending which makes the electron flow easier. Also the plasma may introduced some defect states in the band gap of SiO_2. These states further ease the electron emission.

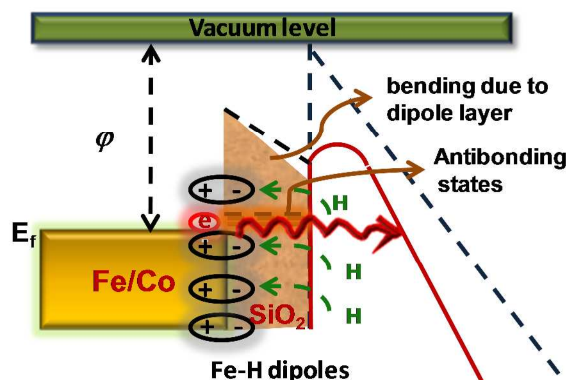

Figure 6: Schematic of electron emission from HPT composite.

The dangling bonds on the surface get chemically terminated by atomic hydrogen. Considering electronegativities, hydrogen is expected to be positive when bonded to Fe or Co. As a result, a dipole moment will set up and hence a potential step will be generated favouring the escape of electrons. Ion etching has generated a large number of defects and has also removed surface oxygen from the top of the metal nanoparticles. Thus, plasma created $Fe^{\delta+}$-$H^{\delta-}$ dipoles[30] and defects modify the surface properties of the composite and lower the work function. In addition, plasma has roughened the surface creating several protrusions which further leads to local field enhancement at the protrusion-tips and hence better field emission properties.

 This journal is © The Royal Society of Chemistry 2012

Table I: Comparison of current density, surface roughness, H count, particle size, effective emissive area and work function of different films. Note that the effective emissive area is not mentioned for those films which show current below 0.45 nA .

Film	Max. Avg. Current Density (μA/cm 2)	r.m.s surface roughness (± 0.05 nm)	H count ($\times 10^{17}$ atoms/cm 2)	Effective emissive area	Particle size (nm)	Work function (eV)
AD	0.5	0.31	Below detection limit	-	-	5.7
200AN	8.1	1.46	1.9	2.0%	6.4	5.2
200HPT	54.2	3.45	3.9	1.7%	10.5	4.8
350AN	2.7	0.95	-	-		5.4
350HPT	1.3	0.50	3.0	-		5.6

Conclusions:

To conclude, H plasma annealing creates $Fe^{\delta+}$-$H^{\delta-}$ dipoles and defects on the surface. The potential drop across this dipole layer has reduced the surface electron affinity by raising the surface band energy. Also the plasma induced anti-bonding states near the Fermi energy level have reduced the overall emission barrier, which is reflected in reduced work function of the HPT200 film. The more occupied VB DOS, enlarged volume of metal nano-clusters inside insulating matrix and increased number of emitting sites on surface together have caused improved FE properties of the same. Increasing the temperature results in out-diffusion of H and agglomeration of particles and reduces the effective emission sites. Thus we envisage that field electron emission efficiency of 200°C hydrogen plasma treated FeCo-SiO_2 nanocomposite thin films make them promising candidates for future applications in nano/micro electronic devices for flat panel displays, high brightness electron source applications.

Acknowledgements

The authors sincerely acknowledge scientific advice and co-operations of Dr. D. K. Avasthi and Dr. D. Kabiraj of IUAC New Delhi for sample preparation, Dr. Saif A. Khan from IUAC and Dr. Ravi Bommali, IIT Delhi for ERDA data analysis. Personnel associated with XPS facility (partially funded by FIST grant of DST) at IIT Delhi are acknowledged. Financial assistance of CSIR, India and experimental facilities at Nano Research Facilities (NRF) IIT Delhi, India are also acknowledged.

Notes and references

[a] Nanostech Laboratory, Department of Physics, Indian Institute of Technology Delhi, New Delhi:110016, India.

1 W. B. Choi, D. S. Chung, J. H. Kang, H. Y. Kim, Y. W. Jin, I. T. Han, Y. H. Lee, J. E. Jung, N. S. Lee, G. S. Park, and J. M. Kim, Appl. Phys. Lett, 1999, **75**, 3129.
2 Y. C. Choi, J. W. Lee, S. K. Lee, M. S. Kang, C. S. Lee, K. W. Jung, J. H. Lim, J. W. Moon, M. I. Hwang, Il H. Kim, Y. H. Kim, B. G. Lee, H. R. Seon, S. J. Lee, J. H. Park, Y. C. Kim and H. S. Kim, Nanotechnology, 2008, **19**, 235306.
3 S. Sridhar, L. Ge, C. S. Tiwary, A. C. Hart, S. Ozden, K. Kalaga, S. Lei, S. V. Sridhar, R. K. Sinha, H. Harsh, K. Kordas, P. M. Ajayan, and R. Vajtai, ACS Appl Mater. Interfaces, 2014, **6**, 1986.
4 B. Zeng, G. Xiong, S. Chen, S. H. Jo, W. Z. Wang, D. Z. Wang, and Z. F. Ren, Appl. Phys. Lett., 2006, **88**, 213108.
5 W.C. Tsai, S.J. Wang, C. L. Chang, C. H. Chen, R.M. K and B.W. Liou, EPL, 2008, **84**, 16001.
6 L. Liao, J. C. Li, D. F. Wang, C. Liu, C. S. Liu, Q. Fu and L. X. Fan, Nanotechnology, 2005, **16**, 985.
7. L. He, Z. Li and Z. Zhang, Nanotechnology, 2008, **19**, 155606.
8 S. Kumar, G. S. Duesberg, R. Pratap, and S. Raghavan, Appl. Phys. Lett., 2014, 105, 103107.
9 D. Pradhan, M. Kumar, Y. Ando and K. T. Leung, Nanotechnology, 2008, **19,** 035603.
10 W.M. Tsang, V. Stolojan, S. P. Wong, J. K. N. Linder, B. J. Sealy and S. R. P. Silva, Rev. Adv. Mater. Sci., 2007, **15,** 179.
11 W. M. Tsang, S. P. Wong and J. K. N. Lindner, Appl. Phys. Lett., 2002, **81**, 3942.
12 C. S. Rout, P. D. Joshi, R. V. Kashid, D. S. Joag, M. A. More, A. J. Simbeck, M. Washington, S. K. Nayak and D. J. Late, 2013, **3**, 3282.
13 D. Sarker, H. Kumar, R. Patra, D. Kabiraj, D. K. Avasthi, S. K. Vayalil, S. V. Roth, P. Srivastava and S. Ghosh. J. Appl. Phys., 2014, **115**, 174304.
14 H. Kumar, S. Ghosh, D. K. Avasthi, D. Kabiraj, N. P. Lalla, T. Shripathi, J. C. Pivin, Vacuum, 2010, **85**, 139.
15 H. Kumar, S. Ghosh, P. Srivastava, D. Kabiraj, D. K. Avasthi, L. Olivi, G. Aquilanti, Adv. Mat. Lett., 2013, **4**, 390.
16 D. Sarker, S. Ghosh, D. Kabiraj, D. K. Avasthi, A. Iadecola, S. K. Vayalil and P. Srivastava. Mater. Research. Express, 2014, **1**, 035017.
17 A. Hart, B. S. Satyanarayana, W. I. Milne and J. Robertson, Appl. Phys. Lett., 1999, **74**, 1594.
18 J. B. You, X. W. Zhang, P. F. Cai, J. J. Dong, Y. Gao, Z. G. Yin, N. F. Chen, R. Z. Wang and H. Yan, Appl. Phys. Lett., 2009, **94**, 262105.
19 C. Y. Zhi, X. D. Bai and E. G. Wang, Appl. Phys. Lett., 2002, **81**, 1690.
20 W. Zhu, G. P. Kochanski, S. Jin, Science, 1998, **282**, 1471.

This journal is © The Royal Society of Chemistry 2012

21 T. Sugino, T. Hori, C. Kimura and T. Yamamoto, Appl. Phys. Lett., 2001, **78**, 3229.

22. B. Zhang, G. Wang, F. Zhang, Y. Xiao and S. Ge, Appl. Phys. A, 2009, 97, 657.

23 H. Kumar, Y. K. Mishra, S. Mohapatra, D. Kabiraj, J. C. Pivin, S. Ghosh, D. K. Avasthi, Nuclear Instruments and Methods in Physics Research B, 2008, **266,** 1511.

24 R. Patra, S. Ghosh, E. Sheremet, M. Jha, R. D. Rodriguez, D. Lehmann, A. K. Ganguli, O. D. Gordan, H. Schmidt, S. Schulze, D. R. T. Zahn and O. G. Schmidtl, J. Appl. Phys., 2014, **115**, 094302.

25 R. H. Fowler, L. Nordheim, Electron Emission in Intense Electric Fields. Proc. R. Soc. Lond. A, 1928, **119**, 173.

26 S. P. Singh, P. Srivastava, S. Ghosh, S. A. Khan and G. V. Prakash, J. Phys. Condens. Matter, 2009, **21** 095010.

27 N. Ishimatsu, T. Shichijo, Y. Matsushima, H. Maruyama, Y. Matsuura, T. Tsumuraya, T. Shishidou, T. Oguchi, N. Kawamura, M. Mizumaki, T. Matsuoka, and K. Takemura, Phys. Rev. B., 2012, **86**, 104430.

28 Krisztina Gajda-Schrantz , Simon Tymen , Florent Boudoire , Rita Toth , Debajeet K. Bora , Wolfram Calvet , Michael Grätzel , Edwin C. Constable and Artur Braun, Phys. Chem. Chem. Phys., 2013, **15**, 1443.

29 J. Stohr and H. C. Siegmann, Magnetism from fundamentals to nanoscale dynamics, Springer.

30 C. Y. Zhi, X. D. Bai, and E. G. Wang, Appl. Phys. Lett., 2002, **81**, 1690.

 This journal is © The Royal Society of Chemistry 2012

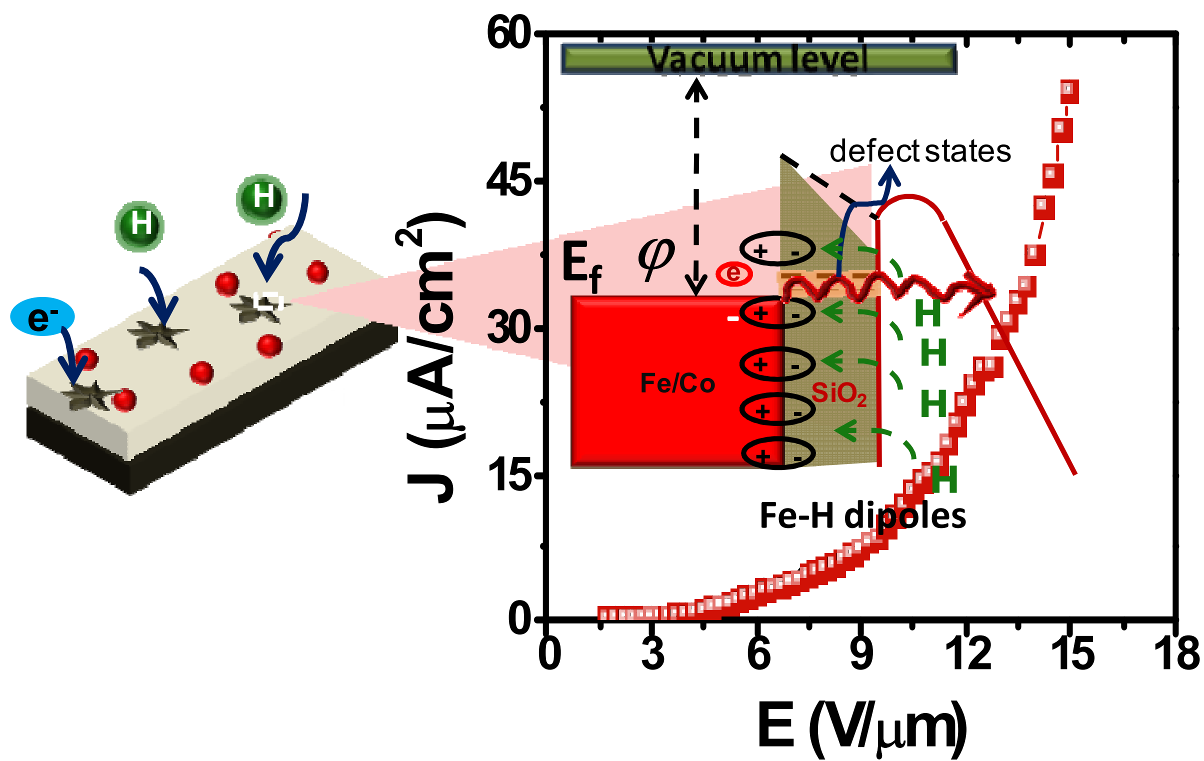

e-
H
H
60
45
30
15
0
0
3
6
9
12
15
18
J (μA/cm2)
E (V/μm)
Vacuum level
defect states
Ef
φ
e
Fe/Co
SiO2
H
H
H
H
Fe-H dipoles